

Xenon gas flow patterns evaluated by high speed multi-row detector CT

Deokiee Chon^a, Ken C. Beck^a, Hidenori Shikata^a, Osama I. Saba^a, Brett A. Simon^b, Chulho Won^a,
and Eric A. Hoffman^a

^aThe University of Iowa, Dept. of Biomedical Engineering, Iowa City, IA 52242

^bThe Johns Hopkins University, Dept. of Anesthesiology, Baltimore, MD 21287

ABSTRACT

Regional lung ventilation can be measured via Xenon-enhanced computed tomography (Xe-CT) by determining washin (WI) and washout (WO) rates of stable Xe. It has been assumed that $WI = WO$, ignoring Xe solubility in blood and tissue and then other geometric issues. We test this by measuring WO-WI in lung by Xe-CT. Also, we investigate the effect of tidal volume (TV) and end inspiratory (EI) vs end expiratory (EE) scan gating on WO and WI measurements. 3 anesthetized, supine sheep were scanned using multidetector-row computed tomography (MDCT). Imaging was gated to both EE and EI during a WI (33 breaths) and WO (20 breaths) maneuver using 55% Xe for WI and room air for WO. Time constants (TCs) of Xe WI and WO were obtained by exponential fitting. WO and WI TCs were compared: 1) apex and base 2) dependent, middle, and nondependent 3) EE and EI 4) three TVs. The vertical gradient of WO-WI showed $WO > WI$ in dependent vs non-dependent regions. WO-WI in both dependent and nondependent region at the lung base and apex was larger when measured at EE compared to EI. As TV increases, the global WO-WI difference decreased. TV showed greater influence on WO than WI. Xe WO was longer than WI possibly reflecting Xe solubility in blood and tissue. Higher TVs and gating to EE provided greater effects on WO than WI TCs which may relate to the number of partial volumed conducting airways contributing to the regional voxel-based measures. We conclude that WO mode is more susceptible to errors caused by either xenon solubility or tidal volume than WI mode and EE scanning may more accurately reflect alveolar ventilation.

Keywords: xenon, wash-out, wash-in, gas solubility, regional ventilation measurements, computed tomography, multi-row detector CT, ventilation, pulmonary imaging, respiratory mode, scanning mode

1.1. INTRODUCTION

In order to develop a theory to comprehend the inert gas exchange at the lung, Kety (10) proposed the model that can be used to measure the regional ventilation and perfusion of the lungs depending on the solubility of inert gas in blood and tissue. According to his model, the regional pulmonary ventilation can be measured by monitoring the rate of washin and/or washout of inert gas, assuming that alveolus is continuously ventilated and the rate of washin of inert gas is the identical to its washout rate. Since xenon (Xe) gas was first introduced by Knipping and his coworkers (11) as contrast material to understand the pulmonary function, it has extensively been used in scintigraphy, magnetic resonance imaging (MRI), single photon emission computed tomography (SPECT), and X-ray (1-3, 5, 16, 18, 22).

Previous studies using Xe scintigraphy reported that due to the solubility of Xe gas in blood and tissue, Xe is absorbed by the blood stream and distributed to the body parts during the washin phase. During the washout phase it then returns to the lung, resulting in a failure to return to the previous baseline, referred to as background activity when using a radioactive tracer (3). Secker-Walker (20) attempted to correct for this background activity by using the washin and washout curves from a region of interest chosen in the basal chest wall. Van der Mark (24) tried to do a background correction by using a model containing a combination of exponential and power series. Both studies, however, were limited in that the Secker-Walker's results depended on the location of the background region of interest and Mark used

a constant background for correction. Gur and his coworkers (reference) later used CT with non-radioactive, radiodense xenon gas (Xe-CT method) to measure regional pulmonary ventilation, taking advantage of the better spatial and temporal resolution of CT, compared to Xe scintigraphy. However, little attention was paid to careful lung volume control and the images presented and suffered from significant misregistration problems

Based upon the assumption on that the rate of washin of Xe gas is the same as the rate of its washout, most previous studies have used three different models interchangeably: washin only, washout only, or combined washin/washout model (5, 14, 21). In this study, we investigate the hypothesis that the washin rate of Xe is identical to its washout rate, using high speed multi-row detector CT. In addition, we investigate the effects of both tidal volume and modes of scan gating (end-inspiratory vs. end-expiratory) on the difference between Xe washin and washout rates.

1.1.1. METHODS

Animal Preparation: This protocol was approved by the University of Iowa Institutional Animal Care and Use Committee. All animal studies were performed within guidelines for animal care adhered to by the American Physiological Society and the N.I.H.

6 adult sheep (30-40 kg) of either sex (3 sheep for protocol 1 and 3 sheep for protocol 2) were studied. Sheep were pre-medicated with I.M. ketamine (1 mg/kg) and acepromazine, anesthetized with isoflurane via a nose cone, a cuffed endotracheal tube (9.0 mm i.d.) placed via tracheotomy, and carotid artery and jugular venous catheters placed via cutdown. Deep anesthesia was maintained with continuous intravenous infusion of propofol (12 mg/kg/hr) drip titrated to heart rate and reflexes. The sheep were mechanically ventilated (10 ml/kg, 12-15 breaths/minute) with a Harvard piston pump respirator.

After instrumentation, the sheep were transported to the scanner facility placed supine on the scanner table, and reconnected to the Harvard respirator. The sheep were relaxed with 0.1 mg/kg pancuronium bromide i.v.. Airway pressure, ECG, end-tidal CO₂ and Xe, and arterial blood pressure were monitored and stored on a computer equipped with an A/D converter board and customized Labview-based PC software. The software was programmed to gate CT imaging based on physiologic information by sending a triggering pulse to the scanner timed to the airway pressure signal. Xenon was delivered via a specialized delivery device (Enhancer 3000, Diversified Diagnostic products, Houston, TX) into the inspiratory port of the ventilator. This device allows for computer control of delivered concentration of Xe and Oxygen gas in a closed circuit using a CO₂ absorber. The sheep were euthanized with and excess of sodium pentobarbital (60 mg/kg i.v.) and concentrated KCl after completion of the study.

Image Specifications: All scan were performed using a multi-detector row CT scanner (MDCT; model MX 8000: Phillips, Cleveland, OH) capable of acquiring 4 simultaneous slices with a gantry rotation speed of 0.5 sec/rotation. For the volume scanning protocol used to locate the position of apex and base slices, the spiral scanning parameters were 100mA, 120kV, slice thickness of 1.3 mm, slice increment of 0.6, scan angle of 180, 225mm field of view, and in plane pixel size of 0.391x0.391 mm. For the multi-breath Xe-CT axial scanning protocol, the scanner was set to 360°, 0.5 sec/rotation, 120 mA, 90 Kv, slice thickness of 2.5mm, 225 mm field of view, and in plane pixel size of 0.449x0.449 mm. For both scanning protocols, 512x512 image matrix and a standard image reconstruction kernel were used.

Xe-CT ventilation protocols: Protocol 1 was designed to assure the existence of background activity in CT scan with a long (4 min) washin and washout times, and to find the optimal number of breaths for the washin period in order to minimize the background activity effects. A series of 130 consecutive end-expiratory CT scans at the lung base were obtained, one image per breath, at the same table location in 3 supine animals. After 7 baseline images were obtained during air breathing, the inspired gas was changed to 55% Xe-25% O₂ in air for a 63 breath-washin period and then switched back to deliver room air for an additional 60 breath-washout period.

Protocol 2 was performed to determine the effects of both tidal volume and scanning mode (end-inspiratory or end-expiratory gating) on the difference between xenon washin and washout rates. A series of 60 consecutive breaths with

both end-inspiratory and end-expiratory gated CT scans was obtained in 3 supine animals: 7 breath baseline, 33 breath Xe-washin, and 20 breath Xe-washout, where the number of washin breaths was determined from the results of protocol 1. Studies were performed at 3 different tidal volumes: 7ml/kg, 10ml/kg, 13ml/kg and both apex and base locations in each animal.

Ventilation Image Analysis: All the images were archived and subsequently analyzed using customized PC software. The lung slice at the first time point was manually segmented from the chest wall and mediastinal structures, and this mask was then applied to all the images in the time series.

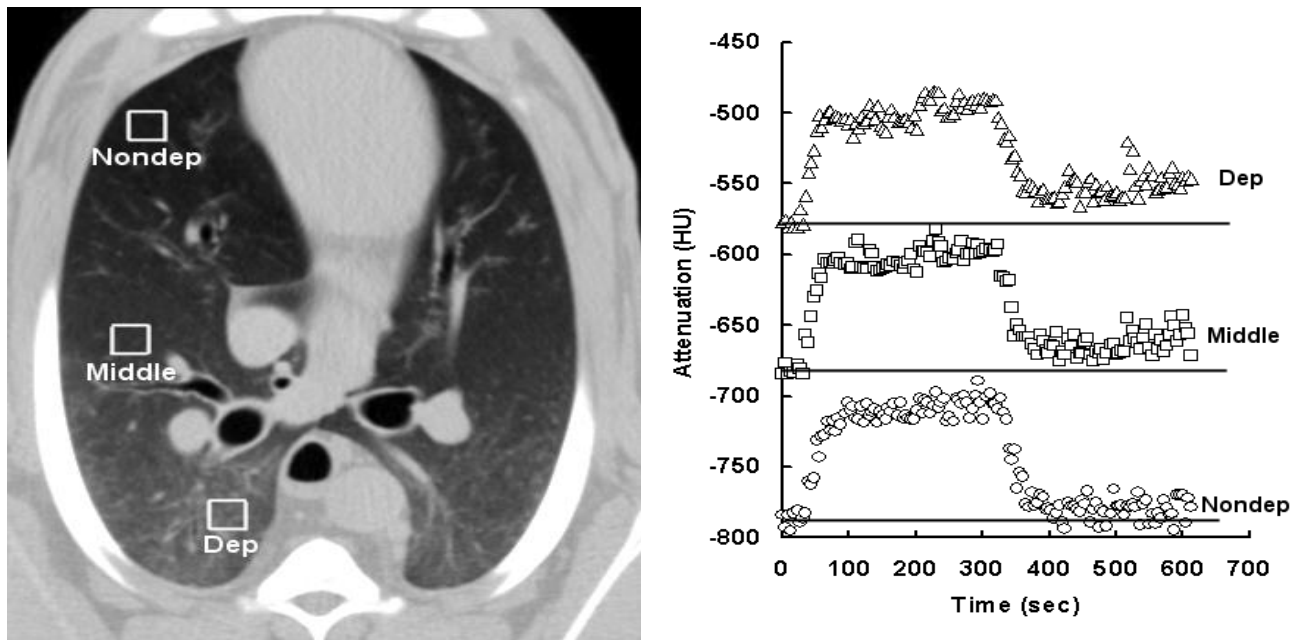


Figure1: Washin and washout in dependent to nondependent regions of one lung Left panel show transverse CT image of a sheep in supine position that contains three ROIs (dependent, middle, nondependent). Right panel shows regional time intensity curve corresponding to 3 ROIs. Initial baselines are displayed at each curve by black horizontal line. From dependent to nondependent ROIs, the difference of initial baseline and the tail of washout curve decrease, indicating incomplete washout in dependent regions.

Figure 1 shows a CT image with 3 regions of interest (ROI) and the ROI density-time curves obtained from the 63 breath Xe-washin and 60 breath washout in one representative sheep. In all 3 regions, the tail of the washout curves did not return to baseline, indicating background activity. The difference between baseline and the tail of washout curve was measured by subtracting the average of the 7 initial pre-Xe time points (initial baseline) from the average of the last 7 time points of washout curve (final baseline), which resulted in the range of 3 to 8 HU in 3 sheep. This result reasonably agrees with the range of 5 - 8 HU Simon et.al. reported under similar conditions with a shorter image series (21).

The increase in Xe after washin and washout is likely due to uptake of Xe in the tissues of the pulmonary and non-pulmonary vascular beds. With slow recirculation of Xe from tissues, washin would be described by an exponential rise to a sloping asymptote. We attempted to minimize the background activity effect by finding the optimal time for the washin phase that allowed completion of washin yet minimized buildup of Xe. To find the optimal washin cutoff time, we calculated the difference between the initial and final baselines, and applied a moving window average operation to find a matching difference on the sloping washin asymptote. A 5 time point average window was moved from the end of washin curve to left by one point. At each movement, the difference between the value of moving window and the

average of the last 5 points of the washin curve was calculated and compared with the difference between initial and final baselines. The window kept moving until the difference calculated was within +/- 1 HU mean difference between initial and final baseline. The cutoff time was determined when the moving window stopped. To minimize the noise, these calculations were performed using the entire lung field in each of 4 image slices from 3 animals. The resulting average of cutoff time was 132+/- 2 (sec) [Mean +/- SD], corresponding to 33 breaths of washin and 15 breath/minute. This result was used in protocol 2.

For the analysis of Xe-CT images in protocol 2, the lung parenchyma was sampled by superimposing a grid with a voxel ROI size of 0.012 cm³ to 0.019 cm³ (5*5 pixels). The mean attenuation for each ROI in each image in the series was measured. Based on the single compartment model, a time constant was calculated for each ROI by separately fitting the washin and washout curves to an exponential function using the Levenberg-Marquardt least-square minimization routine (15). This process enabled the assessment of independent time constants for washin and washout curves of each voxel.

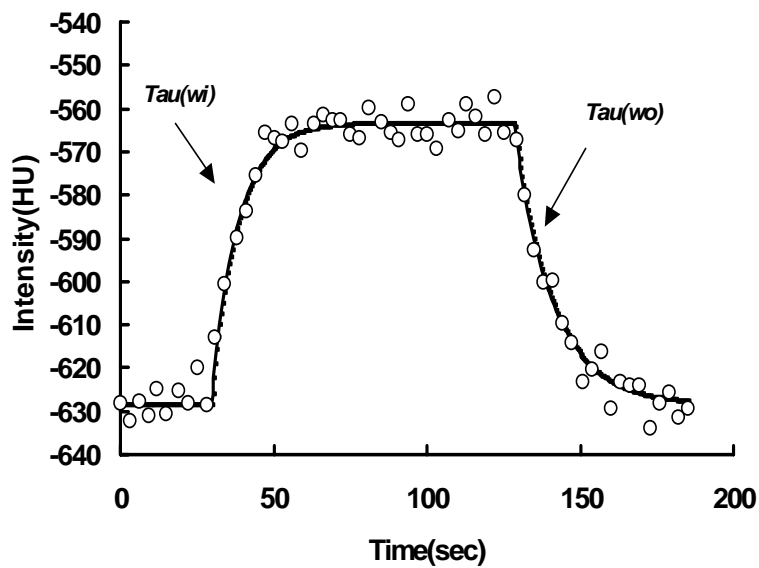


Figure2: Diagram of curve fitting for washin and washout. These curve was obtained by 7 breath baseline, 33 breath washin, 20 breath washout. Note that the tail of washout curve almost reaches to the initial baseline. The time constants for washin [tau(wi)] and washout [tau(wo)] are indicated.

Figure 2 shows one example real washin/washout curve. The model equation and parameters of separated washin and washout curve as follows:

$$D_1(t) = D_0, \quad t < t_0 \quad (1)$$

$$D_2(t) = D_0 + (D_f - D_0) \exp(-[t-t_0]/t) \quad t_0 < t < t_c \quad (2)$$

$$D_3(t) = D_0 + D_2(t_c) \exp(-[t-t_c]/t) \quad t > t_c \quad (3)$$

Where D_0 = the baseline density value, D_f = the density after full equilibration with xenon, t_0 = the time of the beginning of Xe washin, t_c = the time of the beginning of Xe washout (cutoff time). Equation D_1 , D_2 , and D_3 are applied for baseline, xenon washin, and xenon washout curve, respectively. Two different criteria were used to eliminate regions that include major airways and pulmonary blood vessels : voxels with air fraction less than 40% and greater than 90% (7) were eliminated, and regions with SSR (summed squared residual) greater than 150 were eliminated (21).

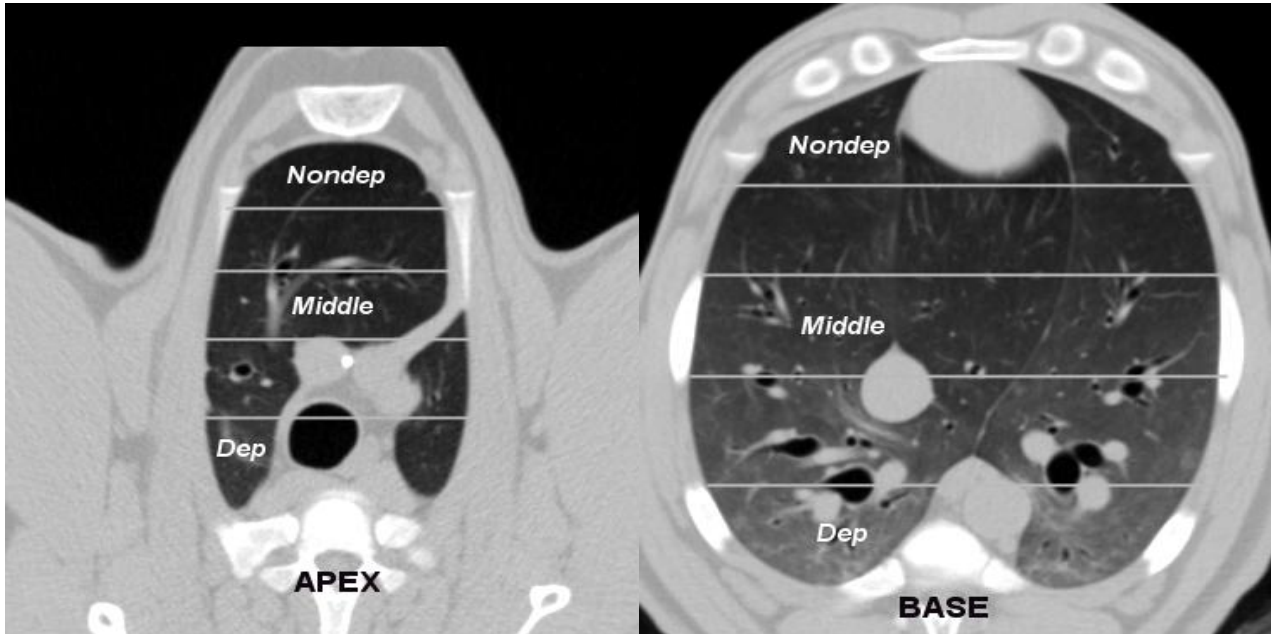


Figure3: Definitions for the three regions at apex and base for the analysis of difference of washin and washout rate. Transverse CT images at apex/base are divided into 5 regions. The most upper part was used as nondependent region, middle part as middle region, and the lowest part as dependent region.

To investigate of the vertical distribution of the difference of xenon washin and washout rate, each slice was divided into 3 regions (figure 3): dependent (lower 20 % of vertical height), middle (middle 20% of vertical height), and nondependent (upper 20% of vertical height). Xenon washin and washout rates for each region were compared: (1) dep vs. nondep, (2) apex vs. base, (3) end-inspiration vs. end-expiration (4) tidal volume at 7ml/kg, 10ml/kg, 13ml/kg.

1.1.2. RESULTS

Xe washin and washout time constants at both apex and base, for dependent and non-dependent regions and comparing end-inspiratory and end-expiratory imaging are summarized in Figure 4. According to the model that Kety (10) proposed, the inverse of this time constant is equal to the regional alveolar ventilation per unit volume, or specific ventilation. At both apex and base, the time constants were shorter in the dependent regions than the nondependent regions, which indicates that dependent regions were better ventilated than nondependent regions at both the apex and base, as expected for a supine animal (14, 19). Time constants for Xe washout were longer than washin at the base and the apex in the dependent location.

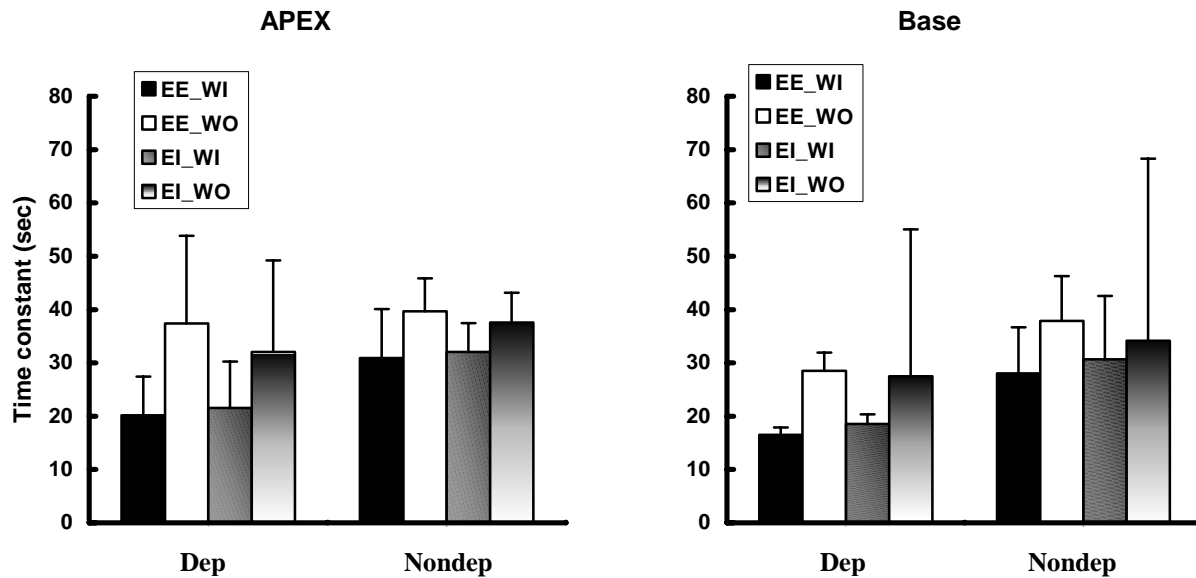


Figure4: Summary data of each washin and washout rate at apex and base, dependent and nondependent by end expiratory and end inspiratory triggering. Note that time constant in nondependent regions is longer than in dependent regions, which means that nondependent regions are less ventilated than dependent regions. This is agreeable with the previous studies.

Table 1 summarizes the averaged washout-washin time constant difference at the apex and base, for 3 different vertical regions (dependent, middle, and nondependent) and with end-inspiratory vs. end-expiratory imaging.

	EE						EI					
	Apex			Base			Apex			Base		
	ND	M	D	ND	M	D	ND	M	D	ND	M	D
1	5.2	4.3	7.0	9.8	5.5	9.8	0.4	0.3	2.0	2.1	3.1	8.0
2	8.7	7.8	27.3	10.8	9.7	26.1	9.6	8.1	19.3	11.9	6.8	20.5
3	12.5	13.3	17.4	12.9	14.9	27.3	6.5	9.8	10.0	8.4	12.3	20.5
Mean	8.8	8.47	17.2	11.1	10.6	21.1	5.5	6.1	10.5	7.5	7.4	16.3
Std	3.6	4.5	10.1	1.6	4.7	9.7	4.7	5.1	8.6	4.9	4.6	7.2

Table 1: Averaged difference of washin and washout rate at three different regions at end expiration and end inspiration. Each number was calculated by averaging the difference of washin and washout in all the voxels in 4 slices that were obtained by filtering it through two criteria: SSR and airfraction.

Each value was calculated by averaging the difference of washin and washout time constants for all the voxels in the 4 simultaneously acquired slices which met SSR and air fraction criteria. Washout-washin time constant differences in dependent regions were bigger than nondependent and middle regions at both the apex and base and with both end-expiratory and end-inspiratory scanning. Note that the difference of washin and washout rates in the middle and nondependent regions were similar. For each region, the differences of washin and washout rates were smaller at the apex than at the base.

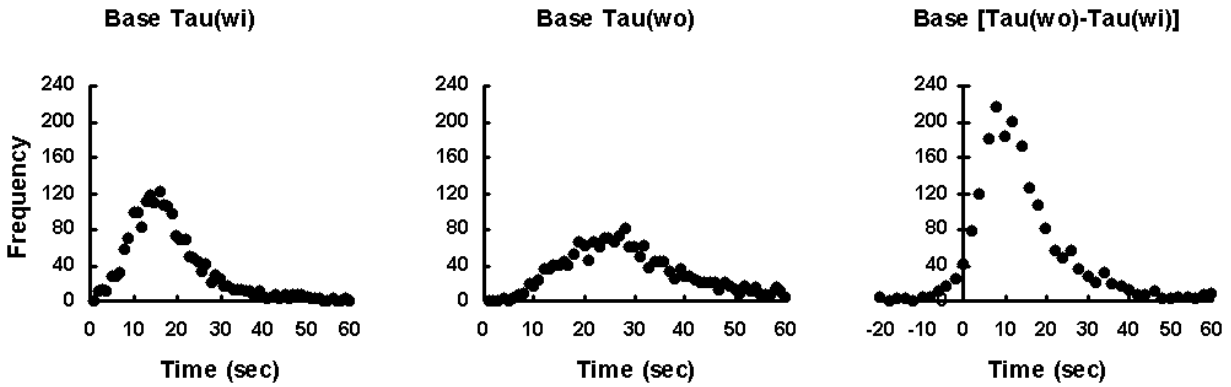


Figure5: Histogram of $\tau(wi)$, $\tau(wo)$, and difference of $\tau(wi)$ and $\tau(wo)$ at base. Note that the distribution of washin time constant is much sharper than washout time constant.

Figure 5 displays the histogram of the difference of the Xe washout and washin time constant at the basal regions of one sheep. The histogram of the differences of time constants between washin and washout was shifted to the right, indicating that the washout time constants are longer than washin. Also, note that the distributions of washin time constants were much sharper than the washout time constant, indicating that washout time constant is less reliable, likely because it is influenced by factors such as the solubility of Xe in blood and tissue.

End Insp vs. End Exp

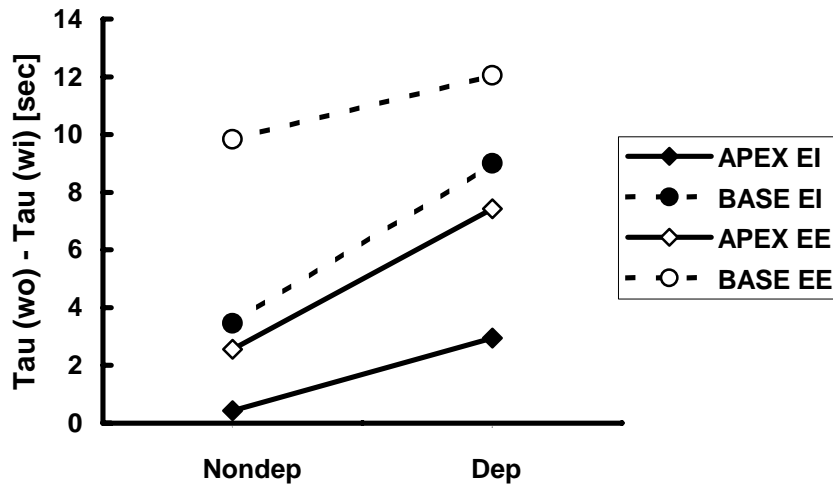


Figure6: Comparison of end inspiration and end expiration at apex/base. At apex and base, difference of $\tau(wi)$ and $\tau(wo)$ is smaller during end inspiratory mode than end expiratory mode.

Difference of xenon washin and washout rate at end inspiratory and end expiratory mode is compared at both apex/base and nondependent/dependent regions, shown in Figure 6. Each point represents the averaged value of the differences of washin and washout rates in 3 sheep. At both apex and base, the difference of washin and washout rates

were smaller with end-inspiratory than end-expiratory imaging, and in the nondependent compared to the dependent regions.

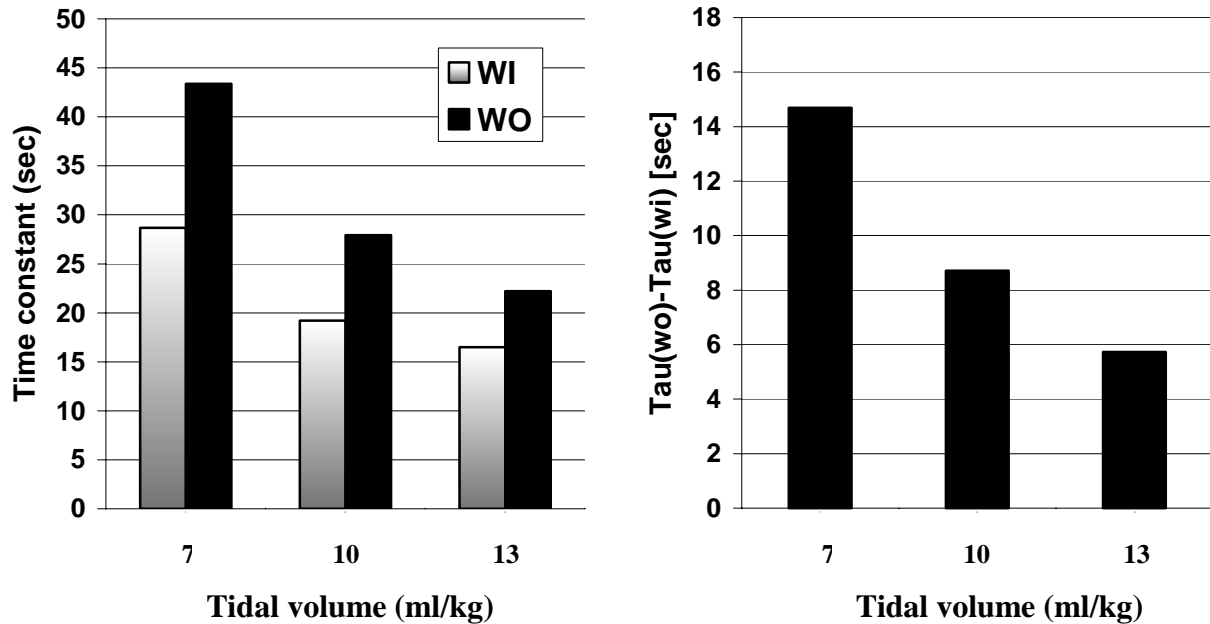


Figure7: Effect of tidal volume on difference of washin and washout rate at base. Each column represents average of 3 sheep. Left panel displays time constant at both washin and washout at 3 tidal volumes. Right panel shows the difference WO-WI at 3 tidal volumes.

Figure 7 shows the effect of tidal volume on difference of xenon washout and washin rates at end expiratory mode for 3 sheep. As tidal volume increases, difference of washout and washin rate decreases at base. Note that the rate of decrease of time constant of washout is greater than washin as tidal volume increases, indicating that washout is more influenced by the change of tidal volume than washin.

1.1.3. DISCUSSION

Xenon gas has been used as a contrast agent for both radioactive and nonradioactive methods in different studies to measure pulmonary ventilation, pulmonary perfusion, the ratio of ventilation and perfusion, cerebral blood flow, and paranasal sinus ventilation (6, 9, 12, 13). Xe is moderately soluble in blood and tissue. The Oswald solubility coefficient is 0.14 at 37°C for blood and 0.13 for fat tissue (8). The solubility of Xe gas has been considered as the one of the sources of errors in the application of multi-breath washin and/or washout protocols. While some of the previous studies tried to correct this error by the assumption of a constant or estimated background signal, others have not used corrections.

Several studies attempting to correct for background activity used the radioactive tracers and a scintillation camera, which has poor spatial and temporal resolution compared to X-ray computed tomography. Secker-Walker and coworkers (20) tried to correct background activity by selecting the large area between and below the lungs and subtracting the average counts/cell derived in the chosen region from each cell in region of interest (ROI). As an index

of lung ventilation, these authors calculated the flow of air per unit volume using the Stewart-Hamilton relationship. They compared the washin and washout rate and showed that washin rate is longer than washout 65.2% before correction. After correction the difference was 7.5%. In the present study, we applied the method of Secker-Walker for correction by choosing a region next to the chest wall to see the difference between washin and washout rate after correction. Our result shows that washout rate is 50% longer than washin before correction and 47.8 % longer than washin after correction. There are several possibilities for why the correction is not as important in our study. One possibility is that while Secker-Walker's study used a scintillation camera with 32x32 matrix as ROI, our study used high temporal and spatial resolution CT with the voxel of 0.012 cm³ to 0.019 cm³. The model we and others used assumed that the region of interest is a homogeneous single compartment, but as the size of ROI is increases, the model may be better explained by a multi-compartment model. The location of the area used for correction may be important. It is possible that partial volume effects and crosstalk between detectors may have caused nuclear scan regions of correction to be contaminated by a lung washin signal.

Another explanation could be that the concentration of Xe used in Secker-Walker study was much lower than the xenon concentration we employed. Our study used a mixture of 55% Xe25% O₂ delivered to sheep, but only a trace of radioactive Xe is administered for scintillation studies. Several studies showed that Xe may affect the determination of respiratory mechanics and especially increase airway pressure due to its higher density and viscosity (4, 27). Thus the use of the lower concentration of Xe may have led to lower airway resistance, which could affect the washin and washout rates as well as the distribution of ventilation.

As the result of the protocol 1, we found 33 breaths of washin as the optimal time point to terminate washin in order to avoid accumulation of Xe in tissues. As the previous studies reported (25), the increase in background activity during washin varied depending on the duration of study, the location and size of ROI, and the subject of study, which appeared to be very complex to find the way of correcting background activity. Instead of trying to correct the background activity after long washin and long washout periods, we made an attempt to prevent the increase in background activity by finding the optimal cutoff time and applying it during subsequent scans.

The averaged difference of washin and washout rates was similar in the middle and nondependent regions, which were smaller than in the dependent regions. Recirculation of Xe gas, taken up by blood flow during washin, stored in the periphery, and then redelivered to the alveoli by the blood during washout, may have contributed to this effect. Since pulmonary blood flow is increased in the dependent regions compared to the middle and the nondependent regions (19), the difference in washin and washout time constants may be enhanced in proportion to the blood flow (26). In addition, the difference of washin and washout rates at the apex was smaller than at the base. This may be explained in part by the distribution of pulmonary of blood flow, as above, which is greater at the base than the apex. Another explanation of the apex-base difference might relate to airway pathway geometry or conductance. Tajik et.al showed that the dorsal, diaphragmatic region of the pig lung receives an enhanced airflow distribution due to the favorable airway structure. This effect favoring flow to the base might be expected to be greater during washin, when the concentration of dense Xe gas is the highest. which would magnify the washin-washout difference.

Figure 6 showed that difference of washin and washout rates with end-expiratory imaging was bigger than with end-inspiratory imaging. Tajik et.al. pointed out that conducting airways are filled with fresh Xe gas at end-inspiration, whereas at end expiration they are filled with alveolar gas. As a result, scanning at end-inspiration causes parenchymal region density to be influenced by partial-volume effects with fresh xenon gas from conducting airways in the ROI (23). Since the effects of recirculation of Xe gas described above involve return of Xe to the alveoli and a small change in alveolar Xe concentration, this may be more evident with end-expiratory imaging which more accurately reflects the alveolar gas composition.

Finally, we demonstrated that as tidal volume increased from 7 to 13ml/kg, the difference between washin and washout rates decreased. One might expect that the greater flow rates associated with higher tidal volumes would increase the effects of differences in regional conductance postulated above, which would tend to increase the differences washout and washin rates. Perhaps the reduction in resistance noted with increasing tidal volumes (17) reduced the regional differences in conductance and thus the difference washin and washout rates.

1.1.4. CONCLUSION

In this study, we found that the WO of xenon gas takes longer than its WI in all 3 lung heights at both apex and base with scans gated both to end expiration and end inspiration. These findings can be, in part, explained by xenon solubility in blood and tissue. Also, we found that tidal volume has an influence on the rates of both retention and clearance of xenon gas. In dependent regions at both apex and base, difference of washin and washout is larger and significantly different in end expiratory scans compared to end inspiratory scans. This can be explained by the hypothesis that fresh xenon/air is inspired into the airway directly and held in the conducting airways during scanning at end whereas the conducting airways are filled with alveolar gas during end expiratory gated scanning. The partial volumed conducting airways in a voxel would then tend to make the difference of washin and washout larger in end expiratory scans than end inspiratory scans. Based on these findings, we conclude that the washout mode is much more susceptible to the error caused by either xenon solubility or tidal volume than the washin mode and scans gated to end expiration may more accurately reflect regional differences in alveolar ventilation.

1.1.5 REFERENCES

1. Almqvist H, Jonson B, Palmer J, Valind S, and Wollmer P. Regional VA/Q ratios in man using ^{133}Xe and single photon emission computed tomography (SPECT) corrected for attenuation. *Clin Physiol* 19: 475-481, 1999.
2. Ball WC, Jr., Stewart PB, Newsham LG, and Bates DV. Regional pulmonary function studied with xenon 133 . *J Clin Invest* 41: 519-531, 1962.
3. Bunow B, Line BR, Horton MR, and Weiss GH. Regional ventilatory clearance by xenon scintigraphy: a critical evaluation of two estimation procedures. *J Nucl Med* 20: 703-710, 1979.
4. Calzia E, Stahl W, Handschuh T, Marx T, Froba G, Bader S, Georgieff M, and Radermacher P. Respiratory mechanics during xenon anesthesia in pigs: comparison with nitrous oxide. *Anesthesiology* 91: 1378-1386, 1999.
5. Gur D, Drayer BP, Borovetz HS, Griffith BP, Hardesty RL, and Wolfson SK. Dynamic computed tomography of the lung: regional ventilation measurements. *J Comput Assist Tomogr* 3: 749-753, 1979.
6. Gur D, Shabason L, Borovetz HS, Herbert DL, Reece GJ, Kennedy WH, and Serago C. Regional pulmonary ventilation measurements by xenon enhanced computed tomography: an update. *J Comput Assist Tomogr* 5: 678-683, 1981.
7. Hoffman EA. Effect of body orientation on regional lung expansion: a computed tomographic approach. *J Appl Physiol* 59: 468-480, 1985.
8. Isbister WH, Schofield PF, and Torrance HB. Measurement of the Solubility of Xenon-133 in Blood and Human Brain. *Phys Med Biol* 10: 243-250, 1965.
9. Kalender WA, Polacin A, Eidloth H, Kashiwagi S, Yamashita T, and Nakano S. Brain perfusion studies by xenon-enhanced CT using washin/washout study protocols. *J Comput Assist Tomogr* 15: 816-822, 1991.
10. Kety SS. The theory and applications of the exchange of inert gas at the lungs and tissues. *Pharmacol Rev* 3: 1-42, 1955.
11. Knipping H, Bolt W, and Venrath H, et al. Eine neue Methode zur Prufung der Herz-und Lungenfunktion. *Dtsch Med Wschr* 80: 1146-1147, 1955.
12. Kreck TC, Krueger MA, Altemeier WA, Sinclair SE, Robertson HT, Shade ED, Hildebrandt J, Lamm WJ, Frazer DA, Polissar NL, and Hlastala MP. Determination of regional ventilation and perfusion in the lung using xenon and computed tomography. *J Appl Physiol* 91: 1741-1749, 2001.
13. Leopold D, Zinreich SJ, Simon BA, Cullen MM, and Marcucci C. Xenon-enhanced computed tomography quantifies normal maxillary sinus ventilation. *Otolaryngol Head Neck Surg* 122: 422-424, 2000.
14. Marcucci C, Nyhan D, and Simon BA. Distribution of pulmonary ventilation using Xe-enhanced computed tomography in prone and supine dogs. *J Appl Physiol* 90: 421-430, 2001.
15. Marquardt D. An algorithm for least-squares estimation of nonlinear parameters. *SIAM* 11: 431-441, 1963.
16. Mishkin FS, Brashear RE, and Reese IC. Evaluation of regional perfusion and ventilation using xenon 133 and the scintillation camera. *Am J Roentgenol Radium Ther Nucl Med* 108: 60-70, 1970.
17. Mols G, Kessler V, Benzing A, Lichtwarck-Aschoff M, Geiger K, and Guttmann J. Is pulmonary resistance constant, within the range of tidal volume ventilation, in patients with ARDS? *Br J Anaesth* 86: 176-182, 2001.

18. Murphy DM, Nicewicz JT, Zabbatino SM, and Moore RA. Local pulmonary ventilation using nonradioactive xenon-enhanced ultrafast computed tomography. *Chest* 96: 799-804, 1989.
19. Musch G, Layfield JD, Harris RS, Melo MF, Winkler T, Callahan RJ, Fischman AJ, and Venegas JG. Topographical distribution of pulmonary perfusion and ventilation, assessed by PET in supine and prone humans. *J Appl Physiol* 93: 1841-1851, 2002.
20. Secker-Walker RH, Hill RI, Markham J, Baker J, Wilhelm J, Alderson PO, and Potchen EJ. The measurement of regional ventilation in man: a new method of quantitation. *J Nucl Med* 14: 725-732, 1973.
21. Simon BA, C. Marcucci, M. Fung, and S. R. Lele. Parameter estimation and confidence intervals for Xe-CT ventilation studies: a Monte Carlo approach. *J Appl Physiol* 84: 709-716, 1998.
22. Swanson SD, Rosen MS, Coulter KP, Welsh RC, and Chupp TE. Distribution and dynamics of laser-polarized (129)Xe magnetization in vivo. *Magn Reson Med* 42: 1137-1145, 1999.
23. Tajik JK, Chon D, Won C, Tran BQ, and Hoffman EA. Subsecond multisection CT of regional pulmonary ventilation. *Acad Radiol* 9: 130-146, 2002.
24. Van der Mark TW, R. Peset, H. Beekhuis, A. E. C. Rookmaker, and M. G. Woldring. An improved method for the analysis of xenon-133 washin and washout curves. *J Nucl Med* 21: 1029-1034, 1980.
25. van der Mark TW, Rookmaker AE, Kiers A, Peset R, Vaalburg W, Paans AM, and Woldring MG. Nitrogen-13 and xenon-133 ventilation studies. *J Nucl Med* 25: 1175-1182, 1984.
26. Won C, Chon D, Tajik J, Tran BQ, Robinswood GB, Beck KC, and Hoffman EA. CT-based assessment of regional pulmonary microvascular blood flow parameters. *J Appl Physiol* 94: 2483-2493, 2003.
27. Zhang P, Ohara A, Mashimo T, Imanaka H, Uchiyama A, and Yoshiya I. Pulmonary resistance in dogs: a comparison of xenon with nitrous oxide. *Can J Anaesth* 42: 547-553, 1995.